AGU PUBLICATIONS

JGR

Journal of Geophysical Research: Oceans

RESEARCH ARTICLE

10.1002/2017JC012925

Key Points:
- Oceanic changes on the Antarctic shelf were examined before and after the calving of Glacier Tongue
- Changes in the intermediate layer are consistent with a regime shift in warm water circulation
- Average decreases in salinity and oxygen isotope ratio might reflect an increase in continental melt

Correspondence to:
S. Aoki,
shigeru@lowtem.hokudai.ac.jp

Citation:
Aoki, S., R. Kobayashi, S. R. Rintoul, T. Tamura, and K. Kusahara (2017), Changes in water properties and flow regime on the continental shelf off the Adélie/George V Land coast, East Antarctica, after glacier tongue calving, *J. Geophys. Res. Oceans, 122*, 6277–6294, doi:10.1002/2017JC012925.

Received 27 MAR 2017
Accepted 18 JUL 2017
Accepted article online 22 JUL 2017
Published online 13 AUG 2017

Changes in water properties and flow regime on the continental shelf off the Adélie/George V Land coast, East Antarctica, after glacier tongue calving

S. Aoki[1,2,3,4], R. Kobayashi[2,5], S. R. Rintoul[3,6], T. Tamura[3,4,7], and K. Kusahara[3]

[1]Institute of Low Temperature Science, Hokkaido University, Japan, [2]Graduate School of Environmental Science, Hokkaido University, Japan, [3]Antarctic Climate and Ecosystems Cooperative Research Centre, University of Tasmania, Hobart, Tasmania, Australia, [4]National Institute of Polar Research, Tokyo, Japan, [5]Now at Marine Works Japan, Yokohama, Japan, [6]CSIRO Oceans and Atmosphere, Hobart, Tasmania, Australia, [7]SOKENDAI, Graduate University for Advanced Studies, Tokyo, Japan

Abstract Oceanic changes before and after the relocation of iceberg B9B and calving of the Mertz Glacier Tongue (MGT) in February 2010 are examined on the continental shelf off the Adélie Land/George V Land coast, East Antarctica. Summer hydrographic observations, including stable oxygen isotope ratio (δ^{18}O), in 2001/2008 and 2011/2015 and results of a numerical model are used. Along the western flank of the MGT, temperature decreased between 2001 and 2015 for most of the water column in the Adélie Depression. δ^{18}O generally decreased, especially at the MGT draft depths on the northern side. West of the MGT, temperature, salinity, and δ^{18}O decreased in the intermediate layer. East of the MGT, in contrast, temperature increased between 2001 and 2011 at intermediate depths, salinity increased in the intermediate and deep layers, and δ^{18}O slightly decreased in the deep layer but did not change much around 300 dbar. The numerical experiment exhibits a change in ocean circulation, revealing an increase in modified Circumpolar Deep Water (mCDW) inflow in the east and a decrease in the west. The contrasting changes in mCDW intrusion are consistent between the observations and numerical model, and are indicative of the effect of removal of the ice barriers. The contrast is overlain by overall decreases in salinity and δ^{18}O, which suggests an increase in the continental meltwater fraction of 5–20% and might reveal a wide-ranging influence from West Antarctica. The oxygen isotope ratio is, hence, effective in monitoring the increase in continental melt over the Antarctic shelf.

Plain Language Summary Antarctic glaciers, icebergs, and ice sheet have significant impact on the surrounding ocean, and, in turn, are affected by the ocean. The Mertz Glacier, East Antarctica, had been melted from below by the oceanic heat. The seaward extension of the glacier of about 500 m tall obstructed sea ice drift from the east and enabled a large amount of sea ice production there. Dense water resulted from the rejected salt was one of the origin of the oceanic abyssal water, which is an important component of the deep ocean circulation. In 2010, however, a drifted iceberg B9B, about the size of Luxembourg, triggered the break of the glacier's terminal. The event caused a drastic change in the ice system, leading to reduction in sea ice production, changes in oceanic water property and oceanic current pathway. Observed oceanic signals indicated the reduction in heat supply from offshore to the west of the glacier extension and increase in the east. The region was also affected by an overall increase in freshwater, which might have been originated from the West Antarctic Ice Sheet. Our results hence propose an importance of monitoring Antarctic ice environment in predicting the global ocean circulation.

1. Introduction

The Antarctic continental shelf is a unique and important region in that it provides very dense water, which is one of the sources of Antarctic Bottom Water (AABW) that fills and spreads to the global abyssal ocean. A significant amount of sea ice is produced off the Adélie and George V Land (AGVL) coast, East Antarctica, centered around the Mertz Polynya [*Tamura et al.*, 2008], and the rejected brine leads to Dense Shelf Water (DSW) formation [*Williams et al.*, 2008]. The DSW exported from the shelf contributes to the formation of

AABW, which makes this region one of a few that contribute to ventilating the abyssal layer [*Rintoul*, 1998]. Hence, oceanic and ice conditions in this region can have a substantial impact on the global meridional overturning circulation (MOC) influencing remote regions through the production of AABW [e.g., *Masuda et al*., 2010].

On the AGVL shelf, water masses are transformed through production of sea ice and interaction with continental ice. During winter, modified Circumpolar Deep Water (mCDW) intrudes from the shelf edge of the Mertz Bank (MB) and is cooled and made more saline by sea ice formation, mainly in the Adélie Depression (AD) [*Williams and Bindoff* 2003] (Figures 1 and 2). The resultant DSW is exported through the Adélie Sill [*Williams et al*., 2008]. The inflow of mCDW on the northern side of the AD and outflow of DSW on the southern side results in a cyclonic circulation in the depression [*Bindoff et al*., 2001; *Williams and Bindoff*, 2003]. Lighter DSW is also exported from the Mertz Depression (MD) to the east [*Williams et al*., 2010]. Ice Shelf Water (ISW) is also present in the AD near the deep portion of the Mertz Glacier Tongue (MGT) [*Williams and Bindoff*, 2003; *Lacarra et al*., 2011], and is indicative of active basal melting underneath the MGT.

The MGT has a large influence on the freshwater budget in the AGVL region. The glacier tongue obstructs the westward movement of sea ice along the shelf, producing an active polynya in its lee that forms and exports large volumes of sea ice and thereby increases the salinity of shelf waters. Melt of the floating glacier tongue supplies freshwater and acts to reduce salinity. Prior to a major calving event in February 2010, the MGT extended across the width of the AD and was grounded at its northwestern tip [*Massom et al*., 2015]. Hence the MGT was a substantial obstacle for ocean circulation on the continental shelf. Movement of the formerly grounded iceberg B9B precipitated the calving of a large portion of the MGT and significant changes to the regional icescape [*Young et al*., 2010]. Sea ice production is thought to have reduced significantly, with estimations based on satellite measurements suggesting a 15–40% reduction in the AGVL region [*Tamura et al*., 2012; *Nihashi and Ohshima*, 2015]. In situ hydrographic observations revealed a significant decrease in salinity at deep and subsurface depths in the AD after the calving event [*Shadwick et al*., 2013; *Lacarra et al*., 2014]. *Lacarra et al*. [2014] suggested that the decrease in deep salinity could be mostly explained by the reduction in sea ice formation. Results of a numerical model revealed a reduction in sea ice production, change in ocean circulation, and a subsequent 23% decrease in DSW export [*Kusahara et al*., 2011].

Numerical models have demonstrated not only a change in sea ice production but also a change in continental ice melting, for different atmospheric and oceanic/ice conditions. *Cougnon et al*. [2013] showed the relationship between sea ice production and basal melting of the MGT for the precalving condition: high (low) sea ice production induces weaker (stronger) intrusion of mCDW and, hence, lower (higher) basal melt rate. *Kusahara et al*. [2016] suggested that the reduction in basal melt rate of the MGT after calving was due to the reduced intrusion of warm mCDW.

Off the AGVL region, long-term changes in AABW properties from the 1970s have been identified [*Jacobs*, 2004; *Aoki et al*., 2005; *Rintoul*, 2007; *Johnson et al*., 2008; *Shimada et al*., 2012] and the trend could be modified after the calving [*Aoki et al*., 2013; *van Wijk and Rintoul*, 2014]. In addition to the abyssal changes, *Aoki et al*. [2013] showed near-surface freshening of winter water and modified shelf water (a mixture of near freezing point shelf water and mCDW) [*Orsi and Wiederwohl*, 2009] at the bottom of the shelf at 140°E for the period 1994–2012, beginning well before the calving event. Therefore, it is likely that different processes acting on different time scales act simultaneously to modify water properties and circulation on the AGVL shelf.

However, hydrographic evidence of water property changes before and after the B9B relocation and MGT calving is still incomplete, especially with regard to the relationship between sea ice production, ice shelf melting, and changes in ocean heat supply. The relationship between sea ice production and DSW in the AD has been investigated, but there has been little study of changes in mCDW and in oceanic conditions in the neighboring regions like the MD. Given the sparseness of existing observations, it is crucial to fully investigate the available hydrographic observations. In particular, the stable oxygen isotope ratio can help to distinguish different contributions to the freshwater budget. The oxygen isotope ratio does not show significant fractionation through the process of sea ice formation, and hence, the ratio in sea ice is similar to that of sea water. However, the oxygen isotope ratio of continental ice is very different from that of sea water and therefore acts as an effective tracer of glacial melt [e.g., *Jacobs et al*., 1985]. The AGVL coast is one

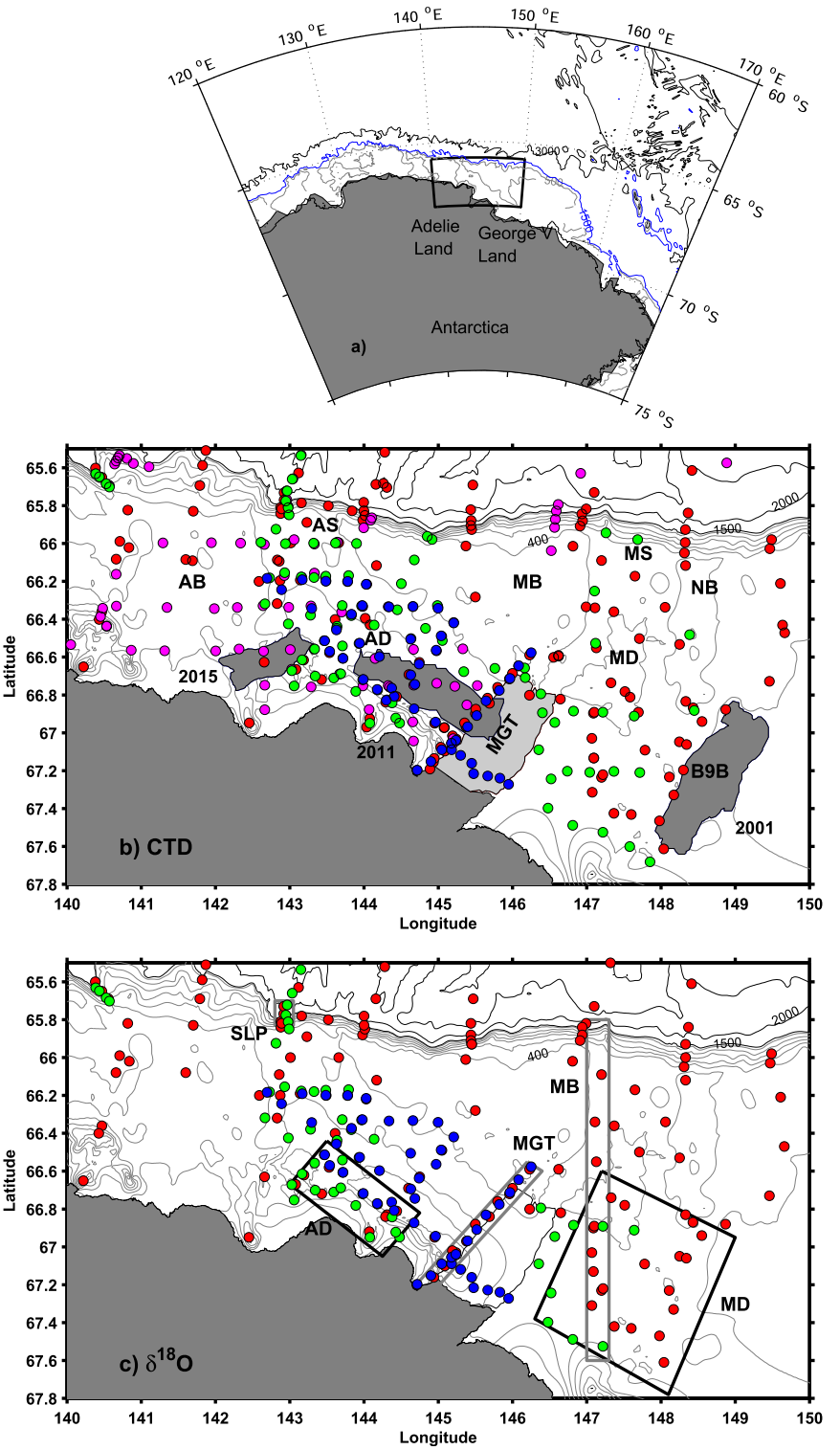

Figure 1. (a) The observation area off the Adélie/George V Land coast, East Antarctica, and location of summertime observations in the Adélie/George V Land shelf region; (b) stations for temperature and salinity, and (**c**) for $\delta^{18}O$. (b and c) Dots denote data from 2001 (red), 2008 (magenta), 2011 (green), and 2015 (blue). Black and gray boxes demarcate the regions and transects used for data comparison. Bathymetry was adopted from IBCSO data [*Arndt et al.*, 2013]. (b) AD denotes Adélie Depression, MD Mertz Depression, AB Adélie Bank, MB Mertz Bank, NB Ninnis Bank, AS Adélie Sill, and MS Mertz Sill. The solid red line denotes the location of the Mertz Glacier Tongue before calving. Solid blue lines indicate the location of B9B in 2001, 2011, and 2015. (c) MGT denotes the transect along the western flank of the Mertz Glacier Tongue, MB Mertz Bank transect along 147°E, SLP Slope transect, AD denotes AD box, and MD MD box.

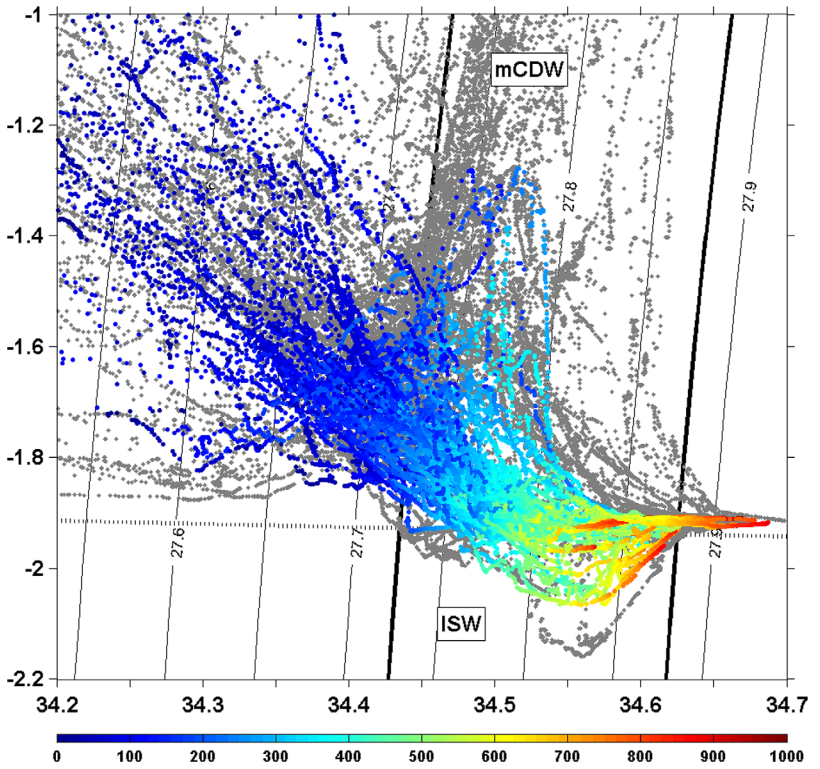

Figure 2. Potential temperature-salinity diagram of the summer time observations (gray dots) in Figure 1a. Colors denote the corresponding depths of the observations, drawn for stations in AD and MD boxes. Dotted line is the freezing point temperature at 50 dbar depth. ISW and mCDW denote the range of Ice Shelf Water and modified-Circumpolar Deep Water, respectively.

of a few regions where high-quality measurements of the stable oxygen isotope ratio have been made over a number of years.

This study aims to clarify the changes in oceanic properties and continental ice melt before and after the B9B relocation and MGT calving in 2010, based on hydrographic surveys, including oxygen isotope ratios, and on satellite observations of sea ice production. Observed changes are compared with the results of a numerical model which reproduces conditions before and after the year 2010.

2 Data and Observational Setting

2.1. Hydrography

To examine broad-scale temporal changes for the AGVL shelf region, top-to-bottom Conductivity-Temperature-Depth profiler (CTD) and stable oxygen isotope ratio observations from 4 years in the period 2001–2015 were examined (Figure 1). For the years 2001, 2011, and 2015, temperature, salinity, and oxygen isotope ratio data were used. Also, CTD data from 2008 were used to supplement the investigation on interannual variability of temperature. The 2001 observations were obtained by RV Nathaniel Palmer and the other data by RSV Aurora Australis. The temperature/salinity data for 2001 and 2008 were collected through the World Ocean Database 2013 (https://www.nodc.noaa.gov/OC5/WOD13/). Data from 2001 and 2008 were used for the precalving period, and those from 2011 and 2015 for the postcalving period.

The stable oxygen isotope ratio of a water sample, with respect to Vienna Standard Mean Ocean Water (VSMOW), is expressed as δ^{18}O, where $\delta^{18}O = \left\{ \frac{\left(\frac{^{18}O}{^{16}O}\right)_{sample}}{\left(\frac{^{18}O}{^{16}O}\right)_{vsmow}} - 1 \right\} \times 1000(‰)$. Water samples for δ^{18}O analysis were not obtained for all stations and bottles due to the limitations in processing (Figure 1b), with the average number of bottles at each station about four in 2001, six in 2011, and eight in 2015. The sampling limitation required spatial averaging of δ^{18}O in the analysis. The 2011/15 samples were processed using a

Finnigan DELTA plus mass spectrometer at ILTS laboratory, Hokkaido University. Measurements for each bottle were duplicated and the precision of the duplicated estimates was estimated to be 0.02‰. The 2001 samples were processed by a FRISON PRISM III mass spectrometer [*Craig*, 1961] with an accuracy of within 0.03‰ [*Jacobs et al*., 2004]. The latter data were obtained from the NASA GISS data set [*Schmidt et al*., 1999].

Temporal differences in δ^{18}O are hence based on data from different laboratories, with the 2001 data from NASA GISS and 2011/2015 data from ILTS, Hokkaido University, and there may be some discrepancy [e.g., *Lippmann et al*., 1999]. To examine the possibility of artifacts due to interlaboratory differences, the nearly colocated δ^{18}O data for the Lower-CDW on the slope, which is the water mass with the least salinity change near this region [*Aoki et al*., 2013], were compared. Five data points in 2001 and seven in 2011, from 700 to 1500 dbar depths except near the bottom, were selected and averaged; the selection was due to the scarcity of data for the same cast, especially in 2001. Average δ^{18}O was -0.138 ± 0.011‰ in 2001 and -0.137 ± 0.021‰ in 2011, while average salinity was 34.676 ± 0.011 and 34.671 ± 0.003, respectively. Although the number of data points is not ideal, the good agreement indicates negligible systematic difference between the two laboratories and, hence, that temporal change is very likely a genuine signal.

To investigate the spatial characteristics of temporal changes, transects and boxes were defined to minimize the effect of different spatial sampling (Figure 1). Three transects were selected, along the western flank of the MGT (MGT), to the east of MGT along 147°E on Mertz Bank (MB), and on the slope around 143°E (SLP), the observations from which covered the periods during 2001–2015, 2001–2011, and 2001–2011, respectively. In addition, two boxes were defined: the AD box is located to the west of the MGT in the AD and MD box to the east of the MGT in the MD.

Although water mass properties differ both in space and time, the upper limit of potential density of mCDW of 1027.725 kgm^{-3} on the shelf corresponded to depth of about 180 dbar in average (Figure 2). DSW was defined as the water denser than 1027.88 kgm^{-3} [*Williams and Bindoff*, 2003], which had the average level of about 650 dbar. We define ISW as water with temperature (hereafter temperature indicates potential temperature) lower than that of the freezing point at 50 dbar [e.g., *Orsi and Wiederwohl*, 2009; *Lacarra et al*., 2011].

2.2. Ice Conditions

Sea ice production derived from satellite microwave measurements was used to infer the contribution of sea ice formation to salinity change [*Tamura et al*., 2008, 2016]. The location of icebergs and the glacier tongue was estimated from previous literature [*Lieser et al*., 2015; *Tamura et al*., 2012], MODIS satellite images (https://worldview.earthdata.nasa.gov/), and the iceberg position tracking record (http://www.scp.byu.edu/data/iceberg/database1. html).

The setting of continental ice in the AGVL region changed drastically over the period of concern. In February 2010, iceberg B9B, which had drifted from the east, triggered the calving of the MGT. Then the terminal part of the MGT, corresponding to 55% of its floating area [*Massom et al*., 2015], broke off and formed new iceberg C28, which had a length of 78 km and width of 35 km. C28 drifted westward and split into two parts at around 140°E, 65.3°S in April 2010, and then drifted out of the area. B9B originated from the Ross Ice Shelf in 1987 and then drifted westward. In 1992, it approached and grounded on the Ninnis Bank, staying there until the end of 2009. After its collision with the MGT, B9B was located around 145°E, 66.8°S in January 2011, then further drifted westward to 143°E after losing some portions, and was still grounded at that location in 2015.

Sea ice conditions and production also changed significantly before and after the calving and relocation event [e.g., *Tamura et al*., 2012; *Nihashi and Ohshima*, 2015]. A region of high sea ice production extended across a broad area west of the MGT before the calving, but was confined to smaller areas near the MGT calving front and west of the fast ice north of the MGT after calving. Before the calving, sea ice production showed significant interannual variability (Figure 3). The years 2002–2003 were characterized by relatively strong polynya activity, while the years 1999–2001 were relatively weak [e.g., *Cougnon et al*., 2013]. The years 2007–2009 were relatively strong. After the calving, sea ice production in the region west of the MGT had decreased to less than half of its former level.

Around the MD, sea ice conditions also changed after the calving event. Fast ice east of the MGT drifted to the west together with B9B in 2010. In 2011, the eastern fast ice had disintegrated, and its area was

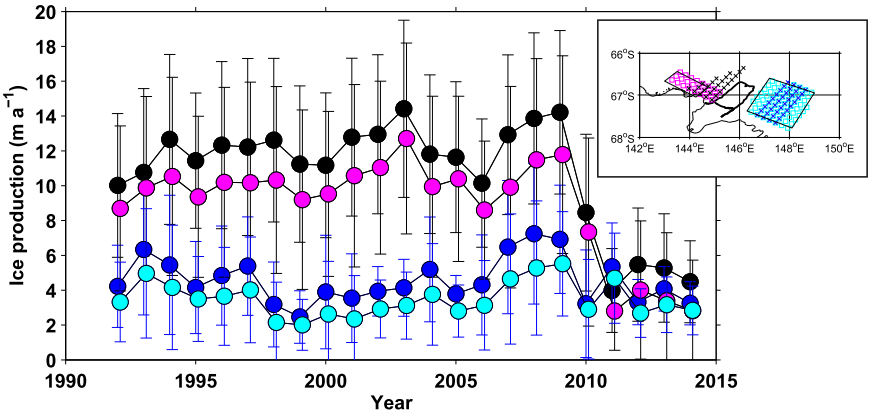

Figure 3. Time series of sea ice production (m a^{-1}) from 1992 to 2014 averaged for the western (magenta and black) and eastern (blue and cyan) regions. Error bars denote the standard deviation within each region. The area-averaged for each color is shown in the inset map.

decreased compared to that before calving. Area-averaged sea ice production to the east of the MGT decreased after calving by a small amount, but the reduction was within the range of interannual variability (Figure 3).

2.3. Numerical Model

The observed signals were interpreted with the results of a coupled ocean/sea ice/ice shelf model [*Kusahara and Hasumi*, 2013, 2014; *Kusahara et al*., 2017]. The numerical model adopts an orthogonal, curvilinear coordinate, which resolves the AGVL region with 5–7 km resolution horizontally and a hybrid σ-/z-coordinate vertically. The freshwater flux from ice shelves to ocean is calculated with a three-equation scheme, based on a pressure-dependent freezing point equation and conservation equations of heat and salinity [*Hellmer and Olbers*, 1989; *Holland and Jenkins*, 1999]. The model was forced by the 40 year ERA-interim surface forcing for 1979–2013. The control run (CTRL) included the MGT, B9B, other icebergs and fast ice in their pre-calving locations. The CTRL run was compared to a run with the regional icescape similar to that observed after the calving event in 2010 (C2000). The differences between the CTRL and C2000 runs were investigated for the climatological average over 13 years to explore the ocean response to changes in the regional icescape [see *Kusahara et al*., 2017 for details]. Although the iceberg settings did not follow a realistic temporal evolution, the basic regimes before/after the calving were incorporated. The global bathymetry for the model was derived from the General Bathymetric Chart of the Oceans (GEBCO) [*IOC et al*., 2003], while ice shelf draft and bathymetry under the ice shelf were obtained from the 1 min refined topography (RTopo-1) data set [*Timmermann et al*., 2010].

3. Results

3.1. Changes in Oceanic Conditions to the West of the MGT

Here we examine the change in water mass properties and distribution along the MGT transect at the western flank of the MGT between 2001 and 2015. The surface layer roughly corresponds to the depth range of 0–150 dbar, the intermediate layer to 150–400 dbar, and the deep layer below 400 dbar.

In 2001, before the calving, a warm mCDW intrusion occurred along the MGT transect at 300–400 dbar, gradually increasing in depth southward from the calving front (Figure 4a). Just below the mCDW layer, the vertical salinity (and density) gradient was strong. Moreover, the depth of the highest vertical salinity gradient also increased gradually toward the coast from about 200 dbar near the calving front to 400 dbar near the southern edge (solid black line in Figure 4b). Below the strong gradient, temperature was rather homogeneous and close to the surface freezing point. A thick layer of ISW (327 ± 190 dbar; the error range denotes standard deviation unless otherwise specified) was found near the Antarctic coast, centered on depths of 400–600 dbar.

In 2015, after the calving, the mCDW intrusion was less evident along the transect. The temperature maximum layer did not extend as far to the south, resulting in cooling of more than 0.5°C near 66.8°S (Figure

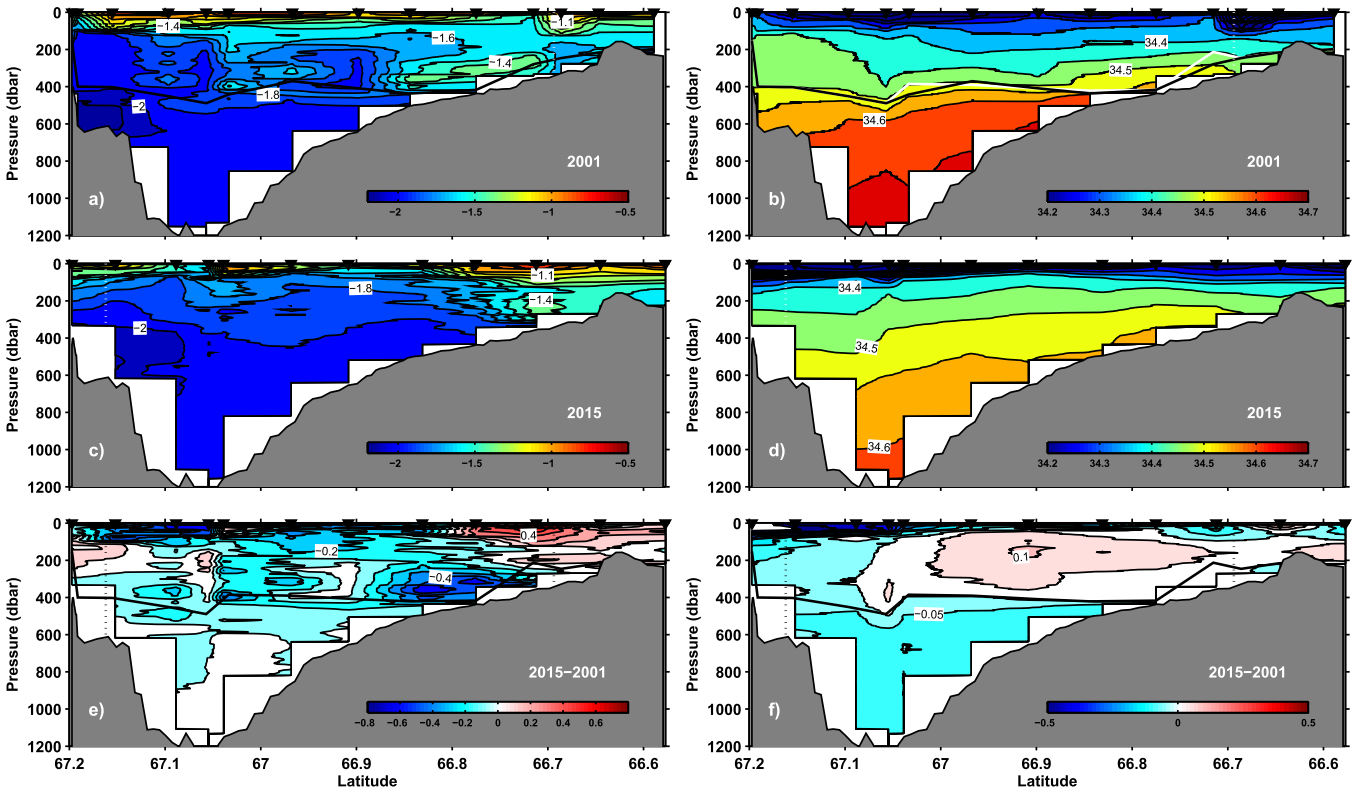

Figure 4. Vertical transects of potential temperature (°C) along the western flank of the Mertz Glacier Tongue in (a) 2001, (c) 2015, and (e) the 2015–2001 difference. Vertical transects of salinity in (b) 2001, (d) 2015, and (f) the 2015–2001 difference. The solid black line in Figures 4a, 4b, 4e, and 4f denotes the level of the highest vertical gradient for salinity below 150 dbar, and the solid white line in Figure 4b denotes that for potential density below 150 dbar. The broken white line denotes the position of the calving front of the Mertz Glacier Tongue. Bathymetry was adopted from IBCSO data [*Arndt et al.*, 2013].

4c). The relatively fresh surface layer was much deeper, and the salinity in the deep trough was higher, in 2001 than in 2015, resulting in stronger vertical gradients of salinity. Between the 2001 calving front location and the deepest part of the AD, the salinity difference (2015 – 2001) was negative (<–0.05) below about 400 dbar (the depth of the strong salinity gradient in 2001) and positive (>0.1) above that depth (Figure 4d). On the southern flank of the AD, the whole column was fresher in 2015, with the strongest freshening and cooling near the surface. The distribution of ISW near the Antarctic coast did not change greatly from that in 2001, but the mean layer thickness decreased to 194 ± 204 dbar.

There were also large differences in δ^{18}O between 2001 and 2015 (Figure 5). In 2001, high δ^{18}O ratios in mCDW (–0.28 to −0.26‰) were detected from the calving front to the northern flank of the AD (Figure 5a). The lowest δ^{18}O (–0.47‰) was observed in the ISW at around 600 dbar at the southern end of the transect, reflecting the influence of basal melting. In 2015, high δ^{18}O was limited to the top of the MB, near the previous calving front, and δ^{18}O was generally lower throughout the transect. The lowest δ^{18}O (–0.46‰) was again found in ISW at around 600 dbar near the Antarctic coast, and similarly low δ^{18}O was found on the northern flank of the AD (Figure 5b). The plot of difference between 2001 and 2015 revealed an overall decrease in δ^{18}O (Figure 5c); the overall mean for each year differed by about −0.05‰. The decrease was largest (∼–0.1‰) at 300–400 dbar depths, where the mCDW signal decreased. A decrease of similar magnitude was found near the surface at the southern side of the AD. A decrease in sea ice production would not normally be associated with a significant decrease in δ^{18}O (it should lead to a negligible increase along the melt-freeze line) [*Craig*, 1961], and hence, the sea ice change cannot explain the overall decrease in δ^{18}O over the AD.

Given the cyclonic circulation in the AD inferred in earlier studies [e.g., *Laccara et al.*, 2011; *Kusahara et al.*, 2011, 2017], the MGT calving might be expected to influence ocean properties and circulation in the western (downstream) region. A significant decrease in the salinity of DSW in the AD has been reported [*Shadwick et al.*, 2013; *Lacarra et al.*, 2014] and related to the decrease in sea ice production [e.g., *Kusahara et al.*,

2011; *Tamura et al.*, 2012]. Here we extend those results, including examination of changes in other water masses and in the distribution of δ^{18}O before and after calving.

In 2001, there was a thick ISW layer along the western flank of the MGT, extending from near the coast across the AD (Figure 6a). Maximum thickness exceeded 500 dbar, and the layer was centered around 400 dbar depth where the MGT left the coast. A thick ISW layer was also found downstream of the MGT in the AD box, with a mean thickness of 172 ± 169 dbar and center depth of 471 dbar for six stations out of nine stations in total, a depth range suggesting an origin at the MGT base. Note that eight stations around B9B in the MD box also revealed ISW, with a mean thickness of 99 dbar and center depth of 443 dbar, indicating the local effect of melting the base of the iceberg. In 2008 the distribution seemed to be generally similar downstream of the MGT, although sampling locations and numbers were limited. One station in the AD box had an ISW thickness of 126 dbar, centered at 370 dbar, out of a total of seven stations. The ISW thickness was hence much greater in 2001 than in 2008, which might be indicative of the interannual variability in the relationship between weaker sea ice production in winter 2000 and subsequent larger basal melt [*Cougnon et al.*, 2013].

In 2011 after the calving, thick ISW was widespread in AD box, which was located downstream of the drifting B9B (Figure 6b), with a mean thickness of 241 ± 149 dbar and a center depth of 594 dbar for 13 stations out of 16 stations in total. The abundance of ISW was probably due to the influence of local melt from B9B

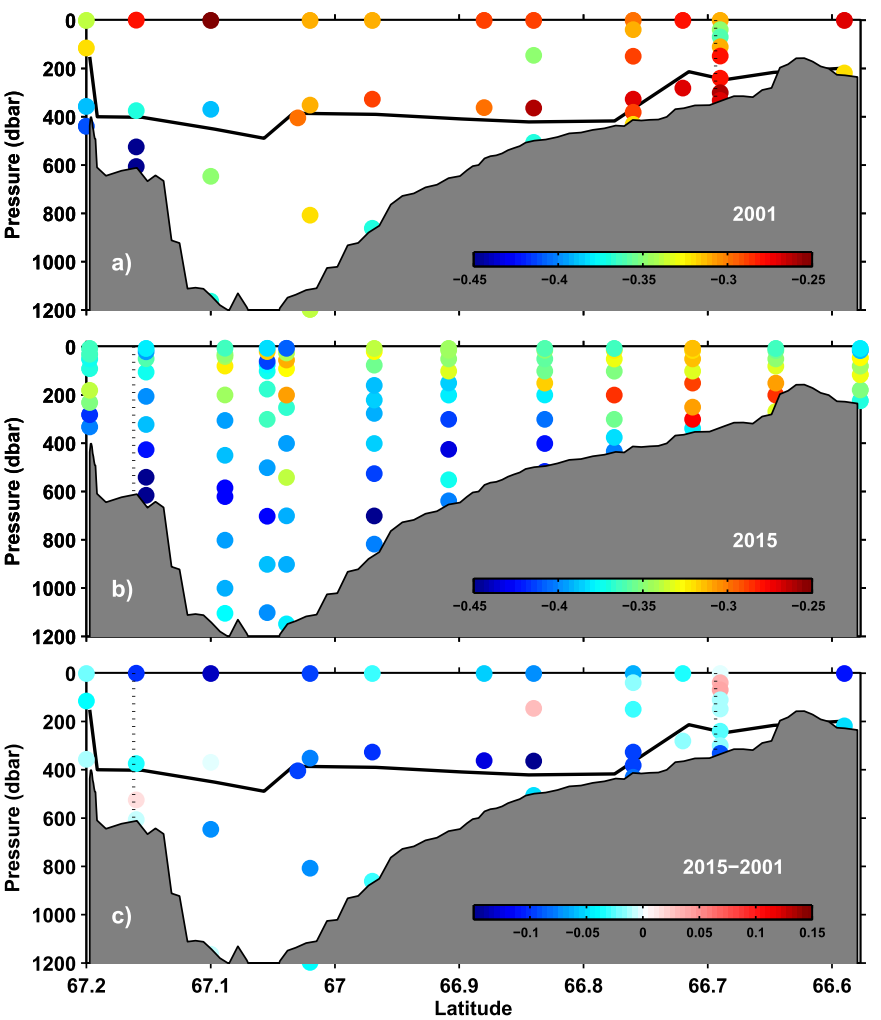

Figure 5. As in Figure 3 but for δ^{18}O (‰) in (a) 2001, (b) 2015, and (c) the 2015–2001 difference. Marker color denotes the δ^{18}O value. In Figure 5c the profiles are derived subtracting 2001 observations, with the 2015 field vertically and linearly interpolated.

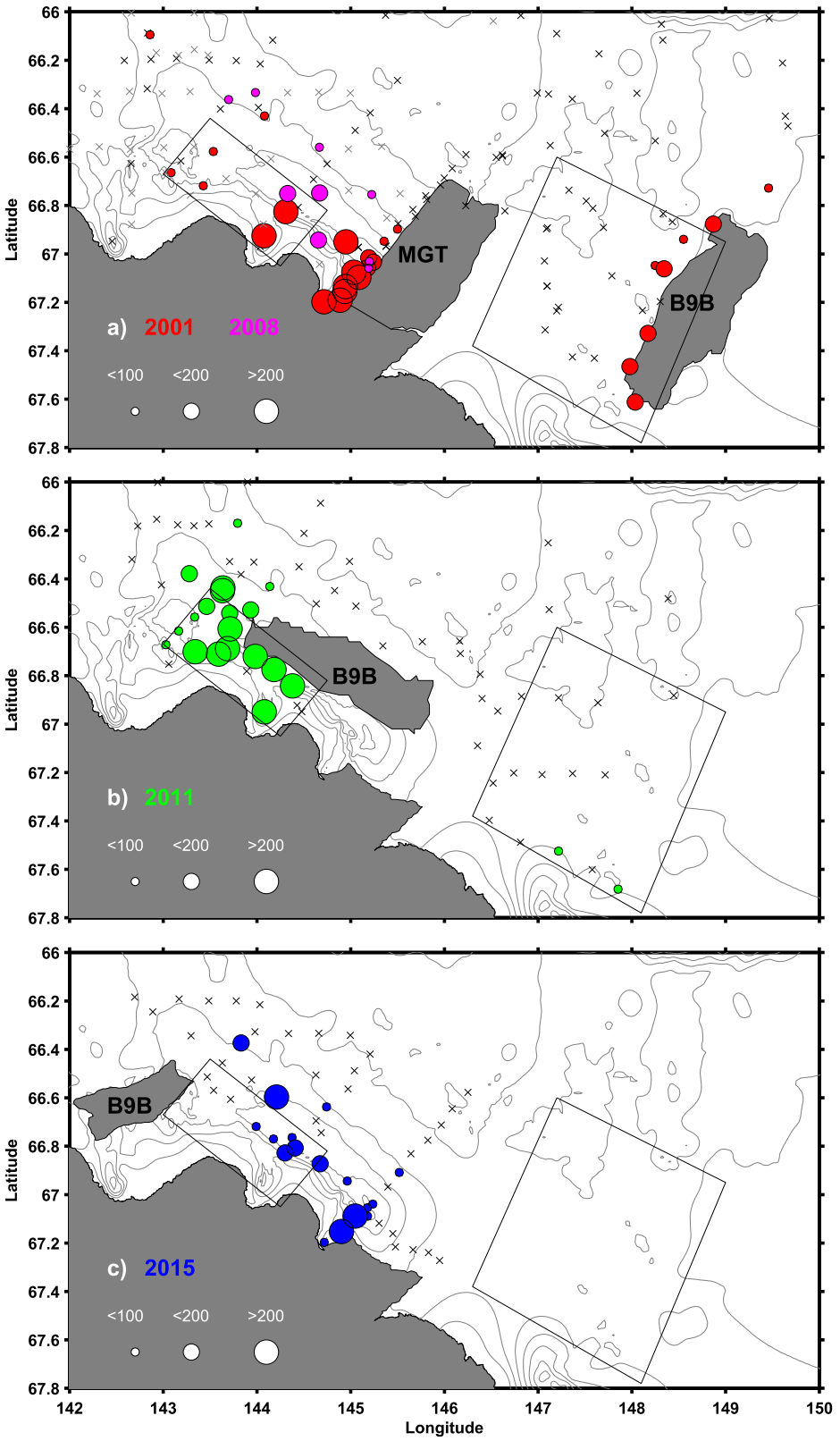

Figure 6. Horizontal distribution of Ice Shelf Water (ISW) layer thickness (in dbar) in (a) 2001 and 2008, (b) 2011, and (c) 2015. The colored dots denote points with ISW (size corresponds to thickness as inset), with red denoting those in 2001, magenta in 2008, green in 2011, and blue in 2015. The black and gray crosses denote points with no-ISW.

overlain onto the signal of MGT origin. Later in 2015, ISW was evident near the new MGT calving front which was close to the mouth of the cavity underneath the MGT (Figure 6c), as also seen in the 2001 MGT transect. ISW was also found in AD box, with a mean thickness of 90 ± 36 dbar and a mean center depth of 499 dbar for five stations out of total eight stations. Hence, assuming the 2011 situation was anomalous due to the local effect of B9B, the amount of ISW in 2015 was not significantly larger than that before the calving; it was less evident compared with that in 2001 and comparable with that in 2008. However, the mean structure may have been influenced by the inhomogeneous sampling, interannual variability, and small-scale factors.

Regional mean temperature and salinity profiles in the AD box revealed different precalving situations in 2001 and 2008 (Figures 7a and 7c). In 2001 temperatures were warmer than in 2008 in the intermediate layers (down to 400 dbar) and salinity was greater (250–600 dbar), suggesting a stronger mCDW signature. Compared with 2001, the mean temperature profile in postcalving 2011/2015 revealed cooling above 400 dbar depth. The column-averaged salinity difference (down to 900 dbar) from 2001 was significantly negative, at -0.050 ± 0.017 in 2011 and -0.045 ± 0.017 in 2015, and the potential density difference was also negative at -0.038 kgm^{-3} in 2011 and -0.035 kgm^{-3} in 2015, consistent with previous studies [*Shadwick et al*., 2013; *Lacarra et al*., 2014]. The temperature and salinity changes between 2001 and 2015 are consistent with those seen on the southern flank of the AD along the MGT transect.

The mean δ^{18}O in the AD box was relatively high at intermediate depths (200–300 dbar) in the mCDW and relatively low at greater depths (400–800 dbar) in the DSW (Figure 8a). δ^{18}O generally decreased between 2001 and 2011/2015. For depth-averaged profiles within 100 dbar-bins, the column mean (for 0–750 dbar) difference was significantly negative, with -0.06 ± 0.05 ‰ in 2011 and -0.06 ± 0.04 ‰ in 2015 (the error range here is derived as the error of the means for each 100 dbar bin). For each year, the decrease was seen throughout the water column with a slight intensification near the surface. As with the western flank of the MGT, the decrease in sea ice production cannot explain the overall decrease in δ^{18}O in this area.

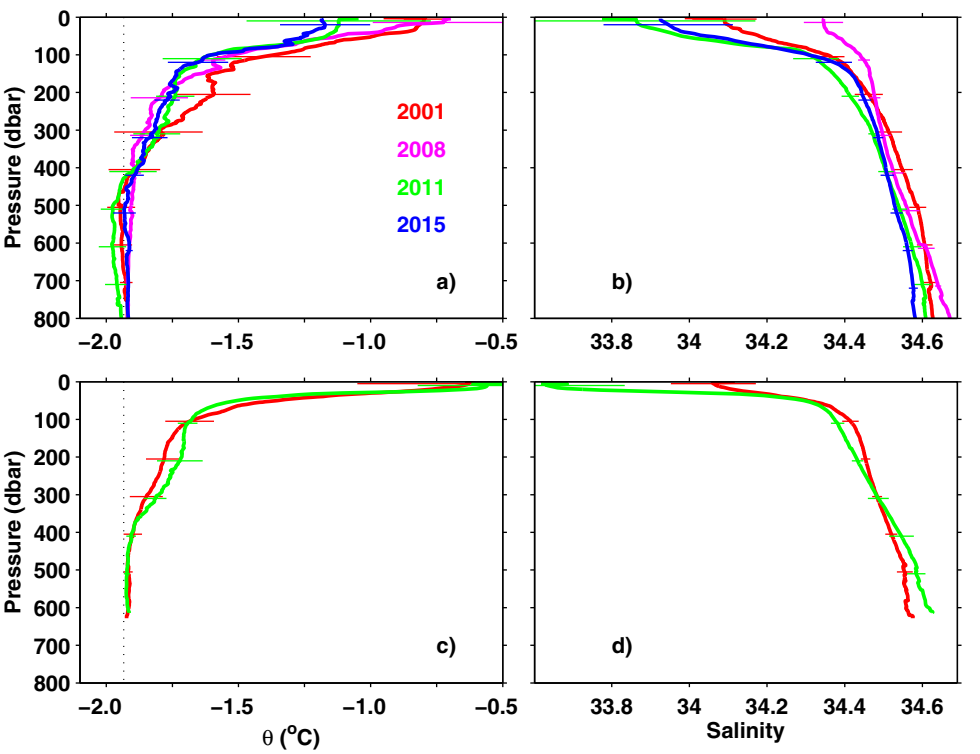

Figure 7. Vertical profiles of area-averaged potential temperature (°C) in (a) AD box and (c) MD box, and of salinity in (b) AD box and (d) MD box. Red lines denote 2001, magenta 2008, green 2011, and blue 2015. Error ranges represent the standard deviation of all observations at a depth. Vertical-dotted line denotes the freezing temperature of a certain salinity (34.55) at 50 dbar depth.

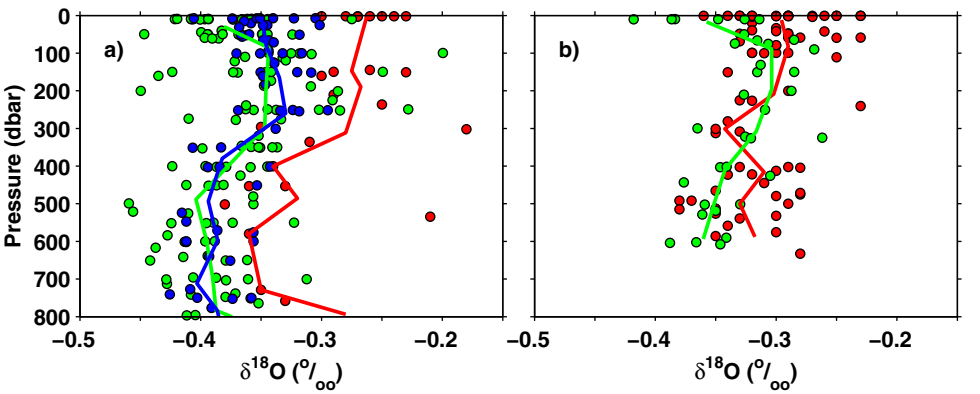

Figure 8. Vertical distribution of observed $\delta^{18}O$ (‰) and vertical bin average profiles in (a) AD box and (b) MD box. Red color denotes 2001, magenta 2008, green 2011, and blue 2015.

3.2. Changes in Oceanic Conditions to the East of the MGT

To the east of the MGT, the loss of B9B and the MGT in 2011 likely created very different oceanic conditions than those in the precalving period. Furthermore, changes in water characteristics between 2001 and 2011 along the eastern transect and in the MD box might not be the same as those observed to the west of the MGT.

Along the MB transect, temperature was close to the surface freezing point deeper than 400 dbar for both 2001 and 2011 on the shelf, indicating the trace of winter convection (Figures 9a and 9c). In 2001, the temperature at intermediate depths (around 200–400 dbar) at 67°S was warmer than that below but significantly cooler than that at the same latitude west of the MGT (Figure 4a), suggesting that intermediate-depth water west of the MGT tip was not directly transported from the east before the calving. Temperature was higher in 2011 than in 2001 in the intermediate level of about100–400 dbar, which corresponded mostly to the mCDW layer. Salinity profiles were more stratified in 2011 than in 2001 (Figures 9b and 9d). Salinity increased in intermediate and deep layers, while it decreased at shallow depths (<250 dbar).

In the MD box, changes in regional mean properties revealed similar tendencies to those along 147°E. Mean temperature in the intermediate layer (150–400 dbar) was higher in 2011 than in 2001, while it was nearly the same near the bottom (Figure 7c). Salinity change varied in the vertical: surface and intermediate depths (0–300 dbar) exhibited a large decrease (–0.053 ± 0.015) that was strongest near the surface, while salinity increased below 300 dbar (by 0.027 ± 0.008; Figure 7d). Accordingly, potential density also increased

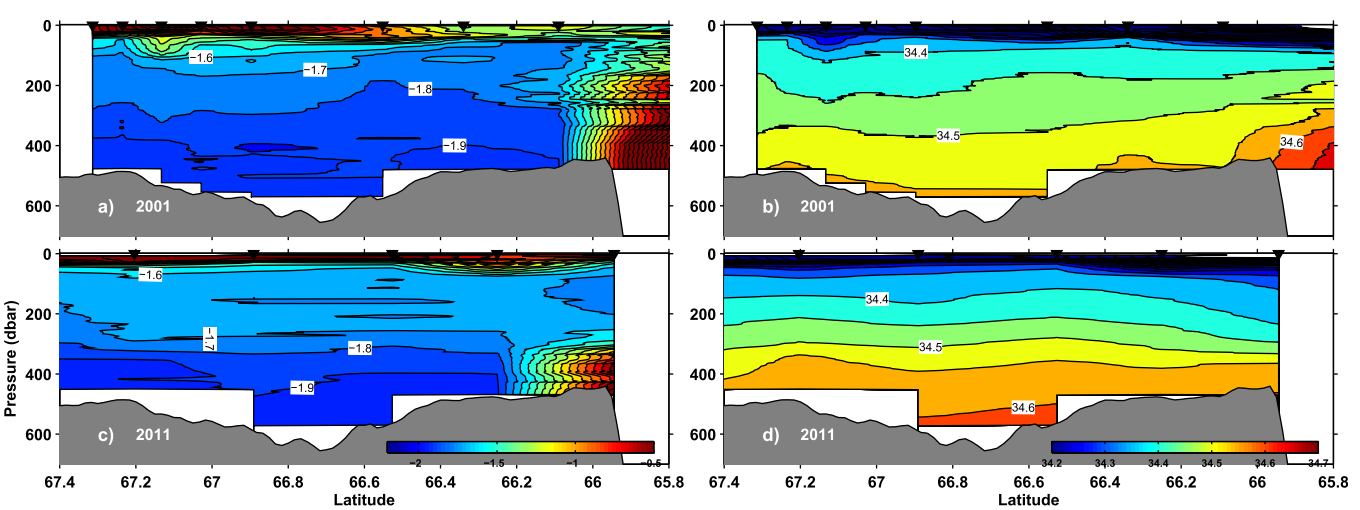

Figure 9. Vertical transects of potential temperature (°C) along 147°E in (a) 2001 and (c) 2011, and of salinity in (b) 2001 and (d) 2011. Bathymetry was adopted from IBCSO data [*Arndt et al.*, 2013].

for the layer deeper than 300 dbar. Column-averaged salinity (0–600 dbar) revealed a slightly negative change (–0.013 ± 0.011).

The column-averaged δ^{18}O in MD box showed an insignificant negative change of $-0.02 \pm 0.04‰$, from $-0.31 \pm 0.03‰$ in 2001 to $-0.33 \pm 0.03‰$ in 2011 (Figure 8b). The decrease was larger near the surface (0–150 dbar) and deep layer (350–650 dbar) but was not evident in the intermediate layer.

The observed increases in temperature and salinity in the intermediate layer are consistent with an increase in mCDW fraction. Sea ice production to the east of the MGT did not significantly differ between 2000 and 2010 (Figure 3), falling within the range of interannual variability. The δ^{18}O change, associated with a salinity increase of 0.027 corresponding to ice production along the melt-freeze line (0.0022‰), was negligible, and hence sea ice change cannot explain the observed decrease in δ^{18}O for the whole water column.

3.3. Changes in Horizontal Contrast West and East of the MGT

As outlined above, the temporal changes have both similar and contrasting aspects in the AD and MD boxes. In both regions, column-averaged salinity and δ^{18}O decreased, and the rate of decrease was larger near the surface. At the same time, salinity in the intermediate to deep layer (from 300 dbar to the bottom) decreased in AD box and increased in MD box, which led to higher salinity in the east than the west after calving. The relative increase in density in the east might also indicate the importance of DSW outflow from the Mertz Sill [*Williams et al*., 2010].

The relationship of δ^{18}O between AD and MD boxes also changed; δ^{18}O was higher in the west in 2001, while it was higher in the east in 2011 (Figures 8 and 10). In 2001, the difference (AD box minus MD box) in the surface dynamic height relative to 600 dbar was negligible (Figure 11). However, in 2011, the difference increased and the dynamic height in the AD box was higher by 0.2 m^2s^{-2}. The height difference induced an increase of westward geostrophic flow toward the Adélie Sill. Hence, the ocean circulation change could be associated with the water property change.

From the δ^{18}O-S diagram, it was clear that δ^{18}O was shifted to lower values from 2001 to 2011/2015 in AD box (Figure 10).The envelope line connecting the δ^{18}O-S properties for the temporal changes has been extrapolated to the line of zero salinity to give the tendency of added freshwater end-member and/or changes in end-member contribution ratio. In the AD box, at the surface (0–50 dbar average) the line through the 2001 and 2011 data extrapolates to a fresh water δ^{18}O of $-31‰$, and that through the 2001 and 2015 data to $-19‰$; the value of the former is close to continental ice and the latter to local precipitation [*Nakamura et al*., 2014]. The envelope for intermediate and deep layers (from 150–650 dbar) is -50 to $-200‰$, which cannot be explained by a simple mixture of known freshwater end-members. In the east, the envelope at the surface is near $-6‰$, which is in between sea ice and local precipitation, and that near the surface (50–150 dbar) is $-21‰$. The layer below 350 dbar shows an increase in salinity, which cannot be explained by an additional input of freshwater end-members. The cause of the property changes, including the contribution of mCDW, will be further examined in the discussion.

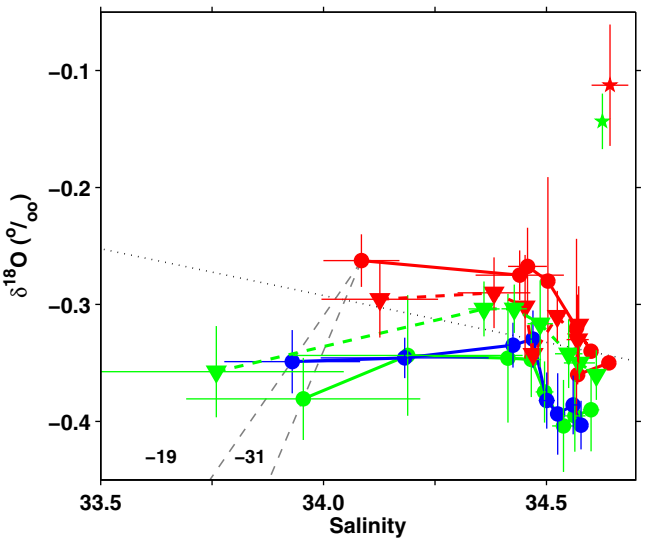

Figure 10. δ^{18}O-salinity diagram for vertical bin-averaged profiles. Dots and solid lines denote AD box profiles, and triangles and dashed lines denote MD box profiles. Stars represent the averaged properties for 400–600 dbar in Slope transect, with red denoting 2001, green 2011, and blue 2015. Error bars for salinity are the depth-averaged standard deviation, and those for δ^{18}O are the standard deviation of 100 dbar bin averages. The dotted line indicates the melt-freeze line [e.g., *Craig*, 1961]. Broken gray lines indicate the envelope of samples pointing to the freshwater end-member with δ^{18}O of $-19‰$ and $-31‰$.

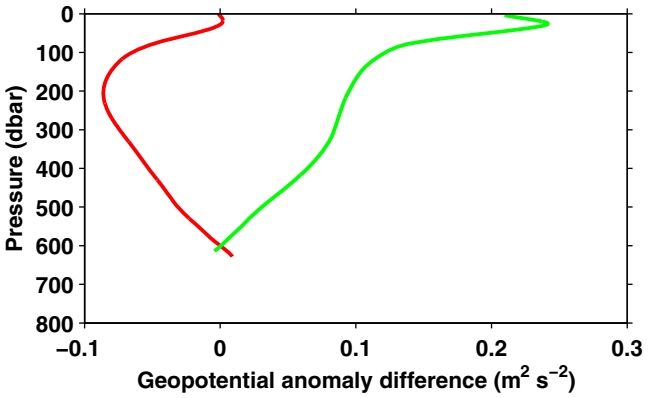

Figure 11. Vertical profiles of the geopotential anomaly spatial difference (West average – East average). Red line denotes 2001 and green 2011.

4. Discussion

4.1. Possible Circulation Change Around the MGT

The changes in observed variables outlined above indicate a contrasting response east and west of the MGT in the intermediate layer; decrease in mCDW was suggested in the AD box while increase was indicated in the MD box. The increase in westward geostrophic shear was also detected, which was consistent with change in ocean circulation. The MGT extended over a vast areal extent both vertically and horizontally and could have acted as a substantial barrier throughout the water column. The depth distribution of the strong salinity gradient along the MGT transect in 2001 (Figure 4b) roughly coincided with the draft depth of the MGT, ranging from 200–300 m near the calving front to 550 m near the coast [*Wang et al*., 2014; *Massom et al*., 2015]. The MGT was grounded at its northwestern tip [*Massom et al*., 2015]. The draft of B9B is also around 400 dbar, judging from the adjacent ISW depth in 2001 and bottom depth at its grounded locations. The Adélie Sill and Mertz Sill, which provide the exit pathways for dense shelf water, have depths of about 400 and 520 dbar, respectively, which is similar to the vertical extent of ice structures like the MGT and B9B. The ice barriers can support a zonal pressure gradient, and without them a stronger zonal flow is possible. Before calving, summer stratification at intermediate depths in the AD [*Lacarra et al*., 2014] was very likely associated with the presence of the MGT. Results of an inverse model, however, did not clearly reproduce a summer circulation difference between 2001 and 2015 [*Snow et al*., 2016]. Detailed analysis focusing on mCDW at the tip of the MGT near the ice barrier is needed to solve the likely contradiction. Given the limitations in spatial and temporal samplings and possible intermittent behavior of mCDW suggested from the Ross Sea observations [e.g., *Kohut et al*., 2013; *Castagno et al*., 2016], comparisons with independent results of numerical models are effective.

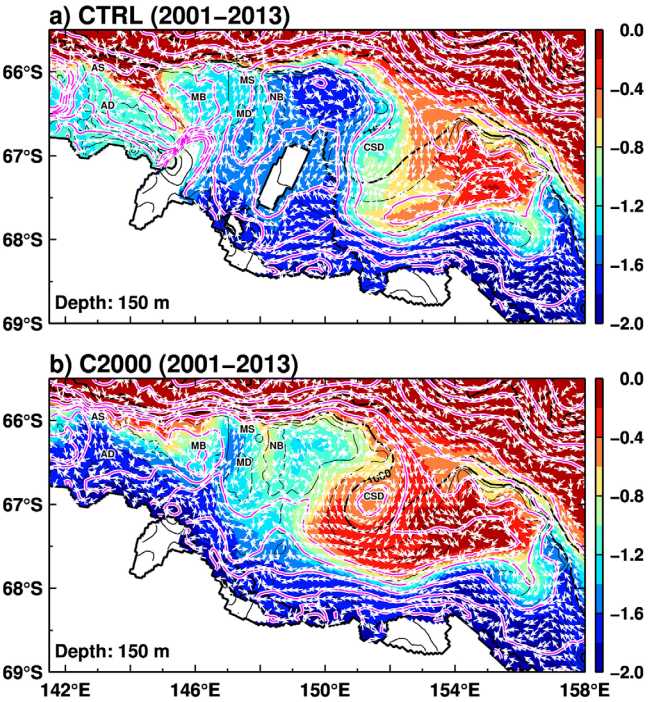

Figure 12. Horizontal distribution of temperature and current vectors at 150 m depth in the numerical model. (a) Control case with the Mertz Glacier Tongue (MGT) and B9B and (b) case without the MGT and B9B.

The numerical experiments carried out in this study reproduced a drastic circulation change before and after the calving event. After calving, there was a decrease in mCDW intrusion along the MB from the Adélie Sill around 144°E, especially in surface and intermediate layers of climatological summer (December–March) average (Figure 12). The reduction in associated heat transport led to cooling in the AD, which is consistent with the observed change from 2001 to 2011/2015 along the MGT transect and in AD box. The numerical model showed a reduction in ISW production after calving, mainly due to reduced heat transport by mCDW. The observational evidence on ISW in the AD box is not conclusive, given the large interannual variability between 2001 and 2008, variable

"icescapes," and low-resolution sampling, but the smaller ISW volume in 2015 than in 2001, a year when the preceding winter sea ice production was weak, supports the conclusion that less mCDW was present after calving, resulting in lower basal melt and lower ISW production. At the same time, the inflow from around 150°E was rerouted from toward shelf edge through the MD to toward the AD. The disappearance of B9B might also have significantly contributed to the pathway change. The observed warming in the intermediate layer is consistent with the numerical model result.

The present model has some limitations. Noted that bathymetry is not satisfactory at some places on the continental shelf, especially around 150°E where no in situ data were available. However, the bathymetry near the Antarctic continent can be comparatively deep to the east of 150°E, judging from the fact that the giant iceberg B9B drifted along the coast until 148.5°E where it grounded. The drift pattern lend support for the prevailing coastal current near the continent. Although a realistic freshwater balance in the AD is difficult to assess (the model reproduced a much warmer mCDW core than observed, and although it reproduced the decrease in sea ice production, bottom salinity in the AD increased due to increased advection from the east), the circulation change is very likely to have contributed to the water mass property change.

4.2. Three End-Member Estimations of Changes in Freshwater Composition

To investigate the cause of the changes in water mass properties, contributions from "meteoric" water, sea ice melt/freeze, and CDW were estimated using the three end-member method with salinity and δ^{18}O [*Meredith et al*., 2008]. The method was applied to the averaged profiles in AD and MD boxes. A negative sea ice fraction contribution indicates sea ice production. Salinity and δ^{18}O values for CDW were estimated as 34.71 ± 0.01 and $-0.034 \pm 0.02‰$ from observations along the continental slope at 3000 m depth. The salinity of sea ice was determined as 5.0 ± 1.1 [e.g., *Eicken*, 1998], and the δ^{18}O as $2.05 \pm 0.20‰$ [e.g., *Melling and Moore*, 1995], the latter from simple extrapolation to the sea ice salinity along the melt-freeze line from the winter water values; notwithstanding that there are large uncertainties in sea ice composition and interannual variability. The "meteoric" component was set to $-30‰$, based on the likely value for the deep portion of continental ice in the surrounding area [e.g., *Stewart*, 1975; *Dansgaard et al*., 1977]. The effect of local precipitation on the "meteoric" component was not considered, assuming that the amount is relatively small and that snow on sea ice tends to drift away from the shelf region. Errors were estimated following a Monte-Carlo approach, with addition of random errors of 10,000 numbers. Although the real errors could be larger, the effect of error can be confined if the discussions are limited to temporal changes and there is no temporal variability in end-member properties.

In the AD box, the meteoric component increased by about 0.2% through almost all the water column (Figures 13a–13c), but with a larger increase near the surface. The higher meteoric component near the surface was consistent with substantial melt of snow and sea ice [*Shadwick* et al., 2013]. The contribution of CDW decreased by 0.11–0.12% for the depth range 50–800 dbar. The change in sea ice component in the deep layer was slightly negative, indicating an increase in production, which is inconsistent with satellite observations. However, the sea ice uncertainty is large, and the significance of this signal is smaller than for the other two components. Given the small signal and large uncertainty in sea ice δ^{18}O, the method might not be an effective indicator of sea ice change.

In the MD box, the meteoric component increased by about 0.05% between 2001 and 2011, except around 300 dbar depth (Figures 13d–13f). The contribution of CDW increased by 0.08% for the depths greater than 300 dbar, while it decreased by 0.13% for shallower depths. The sea ice contribution suggested increased production below 300 dbar and increased melting at shallower depths, although again with a large uncertainty. Hence throughout the AD and MD boxes, meteoric contributions increased, while the CDW contributions revealed contrasting patterns of decrease in the West and increase at depth in the East.

4.3. Source of Excessive Freshwater of Continental Ice Origin

Given the decrease in regionally averaged δ^{18}O and, hence, increase in freshwater with a continental ice component, where does it originate from? Locally, the base and wall of the MGT and/or major icebergs in this region do not seem to be candidates, since the ISW volume near and downstream of the MGT did not show an increase through to summer 2015. Assuming an ISW advective speed of about 20 cms^{-1} [*Bindoff et al*., 2001], the large ISW volume in 2011 should have been flushed out from the depression long before 2015. Although there is no observational evidence from the Ninnis Glacier and Cook Ice Shelf further

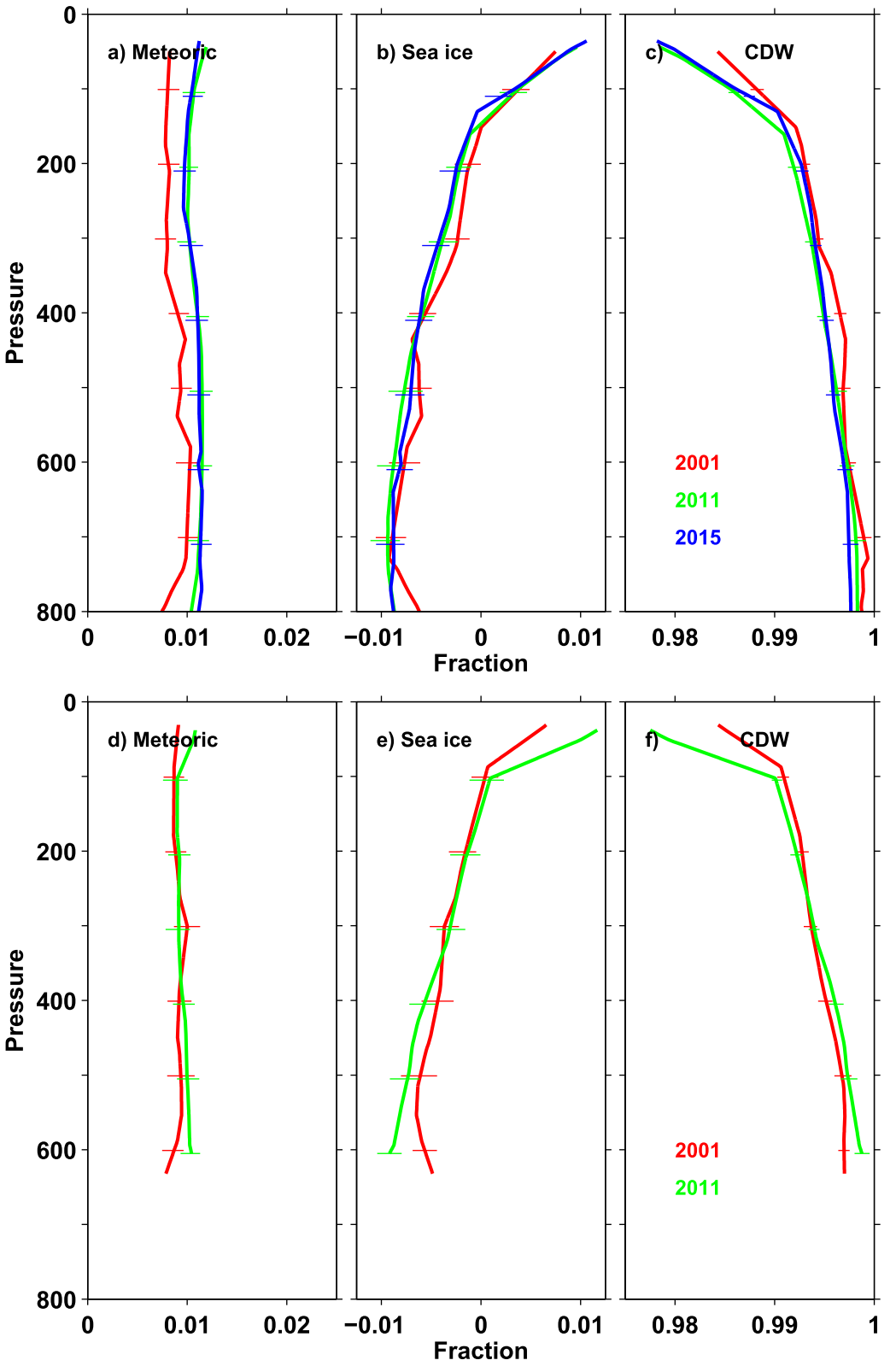

Figure 13. Vertical profiles of the three end-member fractions of (a) meteoric origin, (b) sea ice melt, and (c) Circumpolar Deep Water (CDW) in AD box. Vertical profiles of fractions of (d) meteoric origin, (e) sea ice melt, and (f) CDW in MD box. Error ranges indicate the 90% (two-sided) range, derived from Monte-Carlo method.

upstream, the numerical model result does not point to a significant increase in ice melting for these regions.

A more remote potential source is increased discharge from West Antarctica and its subsequent circumpolar spread [e.g., *Rye et al*., 2014; *Kusahara and Hasumi*, 2013]. If West Antarctica is the source of freshwater, the signal should be detected across a much wider region, including the continental slope. The area for which we can compare past and present δ^{18}O levels is rather limited, but we have nearly colocated data on the upper continental slope along 143°E (Slope transect) in 2001 and 2011. For 400–600 dbar depths where the signal was relatively homogeneous, salinity and δ^{18}O revealed changes of −0.02 and −0.03‰, respectively (star symbols in Figure 10). Further east on the upper continental slope of the Mertz Bank (144–148°E), the salinity change was −0.037 for 50–400 dbar depths, although observations of δ^{18}O were not available. Along 140°E, *Aoki et al*. [2013] reported a similar salinity trend of −0.03 dec^{-1} for winter water (on the slope) and modified shelf water (in D'Urville Trough) for a longer period (1994–2012). The salinity trend of −0.03 dec^{-1} is comparable to those found for shelf waters in the Ross Sea upstream [*Jacobs and Giulivi*, 2010; *Budillon et al*., 2011]. The widespread freshening on the slope might support an offshore advective origin for the additional continental freshwater.

If the freshening from West Antarctica is able to spread almost circumpolar, the overall implication for the freshwater budget is significant. Assuming a homogeneous δ^{18}O change of −0.03‰ dec^{-1}, corresponding to a 0.1% dec^{-1} increase in continental ice fraction, for the 3×10^6 km^2 shelf area shallower than 1000 m isobath and mean depth of 500 m, the continental freshwater increases at a rate of 150 Gtyr^{-1}. Although the estimation is crude and lacks regional variation, it is similar to those proposed for the increasing discharge from West Antarctica [e.g., *Rye et al*., 2014]. In front of the Ross Sea Ice Shelf, salinity and δ^{18}O changes of −0.12 and −0.12‰, respectively, were recorded for the 22 years from 1977–1979 to 2000 [*Jacobs et al*., 2002]. For the shelf off the Antarctic Peninsula, a salinity change of −0.09 was obtained for a 17 year period from 1989 to 2006, which might also include the local effect from the Larsen Ice Shelf [*Hellmer et al*., 2011]. *Schmidko et al*. [2014] detected widespread freshening, except in certain parts of West Antarctica and a part of the Weddell Sea. The freshening with significant δ^{18}O decrease might be part of a widespread freshwater signal originating from West Antarctica, and further evidence from various parts of East Antarctica is necessary to validate this.

5. Conclusions

On the continental shelf off the AGVL coast, significant changes in water mass properties, including δ^{18}O, have been detected during the period between 2001 and 2015. From hydrographic observations and a

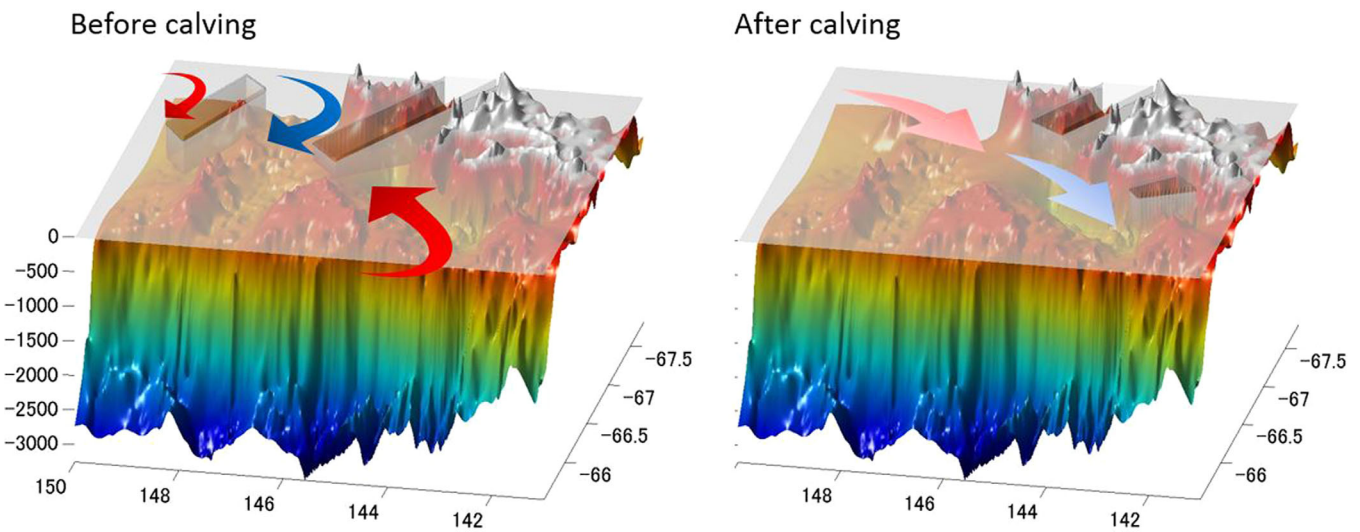

Figure 14. Schematic of circulation patterns before and after the Mertz Glacier Tongue calving. Red arrows denote mCDW intrusion from the continental shelf edge and blue arrows denote mCDW on the shelf with longer residence time. Weaker colors after the calving depict overall freshening effect.

numerical model, contrasting changes between the east and west of the MGT and a possible decrease in ISW volume west of the MGT are consistent with an increase in mCDW intrusion in the east and decrease in the west. The water property changes strongly suggest the striking effect of removing the ice barriers in rerouting the local current system. The contrasting east-west pattern was overlain by area-averaged decreases in salinity and $\delta^{18}O$, which might reflect a widespread increase in the continental meltwater fraction originating from West Antarctica (Figure 14).

As outlined above, ice condition changes including glacier tongue growth and iceberg calving can induce various impacts on oceanic circulation and sea ice production. Oceanic changes associated with variations in heat transport can alter the melt rate of continental ice. For a specific region such as Adélie Depression, these changes can affect the properties of bottom water [*Aoki et al*., 2013], which might influence global MOC. Both sea ice production in coastal polynyas and land-ice conditions such as glacier discharge and iceberg grounding can change the source water properties. A sediment core from this region records a periodicity of around 70 years [*Campagne et al*., 2015], which may be consistent with the cycle of the MGT calving event. Although the present hydrographic evidence is still limited, investigations of upstream freshwater origin and influence also present an important future problem. Given the global impact of changes in Antarctic ice condition, monitoring of the behavior of ice structures is vitally important. $\delta^{18}O$ and salinity observations are effective for estimating the circumpolar spread of freshwater originating from continental ice. Sustained observations, with improved spatial coverage and temporal resolution, will be indispensable.

Acknowledgments

The authors thank Mark Rosenberg, and all officers, crews, and researchers who contributed to the hydrographic observations and water samplings. We are also thankful to Ms. Megumi Kitagawa for her analysing $\delta^{18}O$ samples. CTD data in 2001/2008 data are available through World Ocean Database (https://www.nodc.noaa.gov/OC5/WOD/pr_wod.html) and data in 2011/2015 are through CCHDO (https://cchdo.ucsd.edu/). The $\delta^{18}O$ data in 2001 are provided by NASA/GISS data set (https://data.giss.nasa.gov/o18data/) and those in 2011/15 are available upon request (shigeru@lowtem.hokudai.ac.jp). The Antarctic sea ice production data are available at http://www.lowtem.hokudai.ac.jp/wwwod/polar-seaflux/. This work was supported by JSPS KAKENHI Grant Numbers 25281001 and 17H01615, by the Australian Government's Cooperative Research Centres Program, through the Antarctic Climate and Ecosystems Cooperative Research Centre (ACE CRC), and by the Department of Industry, Innovation, Climate Change, Science, Research and Tertiary Education through the Australian Climate Change Science Program.

References

Aoki, S., S. R. Rintoul, S. Ushio, S. Watanabe, and N. L. Bindoff (2005), Freshening of the Adélie Land bottom water near 140°E, *Geophys. Res. Lett.*, *32*, L23601, doi:10.1029/2005GL024246.

Aoki, S., Y. Kitade, K. Shimada, K. I. Ohshima, T. Tamura, C. C. Bajish, M. Moteki, and S. R. Rintoul (2013), Widespread freshening in the seasonal ice zone near 140°E off the Adélie Land Coast, Antarctica, from 1994 to 2012, *J. Geophys. Res. Oceans*, *118*, 6046–6063, doi:10.1002/2013JC0090009.

Arndt, J. E., et al. (2013), The International Bathymetric Chart of the Southern Ocean (IBCSO) Version 1.0: A new bathymetric compilation covering circum-Antarctic waters, *Geophys. Res. Lett.*, *40*, 3111–3117, doi:10.1002/grl.50413.

Bindoff, N. L., G. D. Williams, and I. Allison (2001), Sea-ice growth and water-mass modification in the Mertz Glacier polynya, East Antarctica, during winter, *Ann. Glaciol.*, *33*(1), 399–406.

Budillon, G., P. Castagno, S. Aliani, G. Spezie, and L. Padman (2011), Thermohaline variability and Antarctic bottom water formation at the Ross Sea shelf break, *Deep Sea Res., Part I*, *58*(10), 1002–1018, http://doi.org/10.1016/j.dsr.2011.07.002.

Campagne, P., et al. (2015), Glacial ice and atmospheric forcing on the Mertz Glacier Polynya over the past 250 years, *Nat. Commun.*, *6*, 6642, doi:10.1038/ncomms7642.

Castagno, P., P. Falco, M. S. Dinniman, G. Spezie, and G. Budillon (2016), Temporal variability of the Circumpolar Deep Water inflow onto the Ross Sea continental shelf, *J. Mar. Syst.*, *116*, 37–49, http://doi.org/10.1016/j.jmarsys.2016.05.006.

Cougnon, E. A., B. K. Galton-Fenzi, A. J. Meijers, and B. Legrésy (2013), Modeling interannual dense shelf water export in the region of the Mertz Glacier Tongue (1992–2007), *J. Geophys. Res. Oceans*, *118*, 5858–5872, doi:10.1002/2013JC008790.

Craig, H (1961), Standard for reporting concentrations of deuterium and oxygen-18 in natural waters, *Science*, *133*, 1833–1834.

Dansgaard, S. J. Johnsen, H. B. Clausen, C. U. Hammer, and C. C. Langway Jr. (1977), Stable isotope profile through the Ross Ice Shelf at Little America V, Antarctica, *Int. Assoc. Hydrol. Sci. Publ.*, *118*, 322–325.

Eicken, H. (1998), Factors determining microstructure, salinity and stable-isotope composition of Antarctic sea ice sea-ice: Deriving modes and rates of ice growth in the Weddell Sea, in *Antarctic Sea Ice Sea-Ice: Physical Processes, Interactions and Variability, Antarct. Res. Ser.*, vol. 74, edited By M. O. Jeffries, pp. 89–122, AGU, Washington, D. C.

Hellmer, H. H., and D. Olbers (1989), A two-dimensional model for the thermohaline circulation under an ice shelf, *Antarct. Sci.*, *1*(4), 325–336.

Hellmer, H. H., O. Huhn, D. Gomis, and R. Timmermann (2011), On the freshening of the northwestern Weddell Sea continental shelf, *Ocean Sci.*, *7*, 305–316.

Holland, D. M., and A. Jenkins (1999), Modeling thermodynamic ice-ocean interactions at the base of an ice shelf, *J. Phys. Oceanogr.*, *29*(8), 1787–1800.

IOC, IHO, and BODC (2003), *GEBCO Digital Atlas, Centenary Edition*. [CD-ROM], Intergovernmental Oceanogr. Comm., Int. Hydrogr. Organ. and Brit. Oceanogr. Data Cent., BODC, Liverpool, U. K. [Available at http://www.gebco.net/data_and_products/gebco_digital_atlas/.]

Jacobs, S. S. (2004), Bottom water production and its links with the thermohaline circulation, *Antarct. Sci.*, *16*, 427–437.

Jacobs, S. S., and C. F. Giulivi (2010), Large multidecadal salinity trends near the Pacific-Antarctic continental margin, *J. Clim.*, *23*(17), 4508–4524, http://doi.org/10.1175/2010JCLI3284.1.

Jacobs, S. S., R. G. Fairbanks, and Y. Horibe (1985), Origin and evolution of water masses near the Antarctic continental margin: Evidence from $H_2^{18}O/H_2^{16}O$ ratios in sea water, in *Oceanology of the Antarctic Continental Shelf, Antarct. Res. Ser.*, vol. 43, edited by S. Jacobs, pp. 59–85, AGU, Washington, D. C.

Jacobs, S. S., C. F. Giulivi, and P. A. Mele (2002), Freshening of the Ross Sea During the Late 20th Century, *Science*, *297*, 386–389, doi:10.1126/science.1069574.

Jacobs, S. S., P. A. Mele, W. M. Smethie Jr., and R. A. Mortlock (2004), *Summer Oceanographic Measurements near the Mertz Polynya (140–150°E) on NB Palmer Cruise 00–08, LDEO-2003–3*, Lamont-Doherty Earth Observ. of Columbia Univ., Palisades, N. Y.

Johnson, G. C., S. G. Purkey, and J. L. Bullister (2008), Warming and freshening in the Abyssal Southeastern Indian Ocean, *J. Clim.*, *21*, 5351–5363.

Kohut, J., E. Hunter, and B. Huber (2013), Small-scale variability of the cross-shelf flow over the outer shelf of the Ross Sea, *J. Geophys. Res. Oceans*, *118*, 1863–1876, http://doi:10.1002/jgrc.20090.

Kusahara, K., and H. Hasumi (2013), Modeling Antarctic ice shelf responses to future climate changes and impacts on the ocean, *J. Geophys. Res. Oceans*, *118*, 2454–2475, doi:10.1002/jgrc.20166.
Kusahara, K., and H. Hasumi (2014), Pathways of basal meltwater from Antarctic ice shelves: A model study, *J. Geophys. Res. Oceans*, *119*, 5690–5704, doi:10.1002/2014JC009915.
Kusahara, K., H. Hasumi, and G. D. Williams (2011), Impact of the Mertz Glacier Tongue calving on dense water formation and export, *Nat. Commun.*, *2*, 159, doi:10.1038/ncomms1156.
Kusahara, K., H. Hasumi, A. D. Fraser, S. Aoki, K. Shimada, G. D. Williams, R. Massom, and T. Tamura (2017), Modeling ocean-cryosphere interactions off Adélie and George V Land, East Antarctica, *J. Clim.*, *30*, 163–188, doi:10.1175/JCLI-D-15-0808.1.
Lacarra, M., M.-N. Houssais, E. Sultan, S. R. Rintoul, and C. Herbaut (2011), Summer hydrography on the shelf off Terre Adélie/George V Land based on the ALBION and CEAMARC observations during the IPY, *Polar Sci.*, *5*, 88–103.
Lacarra, M., M.-N. Houssais, C. Herbaut, E. Sultan, and M. Beauverger (2014), Dense shelf water production in the Adélie Depression, East Antarctica, 2004–2012: Impact of the Mertz Glacier calving, *J. Geophys. Res. Oceans*, *119*, 5203–5220, doi:10.1002/2013JC009124.
Lieser, J. L., R. A. Massom, and P. Heil (2015), Sea ice reports for the Antarctic shipping season 2014–2015, Antarct. Clim. and Ecosyst. Coop. Res. Cent., Hobart, Tasmania.
Lippmann, J., M. Gröning, and K. Rozanski (1999), 2nd Interlaboratory comparison for deuterium and oxygen-18 analysis of water samples, Isotope Hydrology Laboratory Agency's Laboratories Seibersdorf, 40 pp., Int. At. Energy Agency, Vienna.
Massom, R. A., A. B. Giles, R. C. Warner, H. A. Fricker, B. Legrésy, G. Hyland, L. Lescarmontier, and N. Young (2015), External influences on the Mertz Glacier Tongue (East Antarctica) in the decade leading up to its calving in 2010, *J. Geosphys. Res. Earth Surf.*, *120*, 490–506, doi:10.1002/2014JF003223.
Masuda, S., et al. (2010), Simulated rapid warming of abyssal north pacific waters, *Science*, *329*, 319–322.
Melling, H., and R. M. Moore (1995), Modification of halocline source waters during freezing on the Beaufort Sea shelf: Evidence from oxygen isotopes and dissolved nutrients, *Cont. Shelf Res.*, *15*, 89–113.
Meredith, M. P., M. A. Brandon, M. I. Wallace, A. Clarke, M. J. Leng, I. A. Renfrew, N. P. M. van Lipzig, and J. C. King (2008), Variability in the freshwater balance of northern Marguerite Bay, Antarctic Peninsula: results from $\delta^{18}O$, *Deep Sea Res., Part II*, *55*, 309–322.
Nakamura, K., S. Aoki, K. Yoshimura, and N. Kurita (2014), Distribution of oxygen isotope ratio of precipitation in the Atlantic-Indian sectors of the Southern Ocean, *SOLA*, *10*, 154–157, doi:20.2151/sola.2014-032.
Nihashi, S., and K. I. Ohshima (2015), Circumpolar mapping of Antarctic coastal polynyas and landfast sea ice: Relationship and variability, *J. Clim.*, *28*, 3650–3670, doi:10.1175/JCLI-D-14-00369.1.
Orsi, A. H., and C. L. Wiederwohl (2009), A recount of Ross Sea waters, *Deep Sea Res., Part II*, *56*, 778–795.
Rintoul, S. R. (1998), On the origin and influence of Adélie Land Bottom Water, in *Ocean, Ice and Atmosphere: Interactions at Antarctic Continental Margin, Antarct. Res. Ser.*, vol. 75, edited by S. S. Jacobs and R. Weiss, pp. 151–171, AGU, Washington, D. C.
Rintoul, S. R. (2007), Rapid freshening of Antarctic Bottom Water formed in the Indian and Pacific oceans, *Geophys. Res. Lett.*, *34*, L06606, doi:10.1029/2006GL028550l.
Rye, C. D., A. C. Naveira Garabato, P. R. Holland, M. P. Meredith, A. J. Nurser, J. George, C. W. Hughes, A. C. Coward, and D. J. Webb (2014), Rapid sea-level rise along the Antarctic margins in response to increased glacial discharge, *Nat. Geosci.*, *7*(10), 732–735, doi:10.1038/ngeo2230.
Schmidko, S., K. J. Heywood, A. F. Thompson, and S. Aoki (2014), Multi-decadal warming of Antarctic waters, *Science*, *346*(6214), 1227–1231, doi:10.1126/science.1256117.
Schmidt, G. A., G. R. Bigg, and E. J. Rohling (1999), "Global Seawater Oxygen-18 Database: v1.21", Goddard Institute of Space Studies, NASA, N. Y. [Available at http://data.giss.nasa.gov/o18data/.]
Shadwick, E., et al. (2013), Glacier tongue calving reduced dense water formation and enhanced carbon uptake, *Geophys. Res. Lett.*, *40*, 904–909, doi:10.1002/grl.50178.
Shimada, K., S. Aoki, K. I. Ohshima, and S. R. Rintoul (2012), Influence of Ross Sea Bottom Water changes on the warming and freshening of the Antarctic Bottom Water in the Australian-Antarctic Basin, *Ocean Sci.*, *8*, 419–432.
Snow, K., B. M. Sloyan, S. R. Rintoul, A. McC. Hogg, and S. M. Downes (2016), Controls on circulation, cross-shelf exchange, and dense water formation in an Antarctic polynya, *Geophys. Res. Lett.*, *43*, 7089–7096, doi:10.1002/2016GL069479.
Stewart, M. K. (1975), Hydrogen and oxygen isotope studies on the McMurdo Ice Shelf, Antarctica, *N. Z. J. Geol. Geophys.*, *18*, 49–64.
Tamura, T., K. I. Ohshima, and S. Nihashi (2008), Mapping of sea ice production for Antarctic coastal polynyas, *Geophys. Res. Lett.*, *35*, L07606, doi:10.1029/2007GL032903.
Tamura, T., G. D. Williams, A. D. Fraser, and K. I. Ohshima (2012), Potential regime shift in decreased sea ice production after the Mertz Glacier calving, *Nat. Commun.*, *3*, 826, doi:10.1038/ncomms1820.
Tamura, T., K. I. Ohshima, A. D. Fraser, and G. D. Williams (2016), Sea ice production variability in Antarctic coastal polynyas, *J. Geophys. Res. Oceans*, *121*, 2967–2979, doi:10.1002/2015JC011537.
Timmermann, R., et al. (2010), A consistent data set of Antarctic ice sheet topography, cavity geometry, and global bathymetry, *Earth Syst. Sci. Data*, *2*, 261–273, doi:10.5194/essdd-3-231-2010.
van Wijk, E. M., and S. R. Rintoul (2014), Freshening drives contraction of Antarctic Bottom Water in the Australian Antarctic Basin, *Geophys. Res. Lett.*, *41*, 1657–1664, doi:10.1002/2013GL058921.
Wang, X. W., X. Cheng, P. Gong, C. K. Shum, D. M. Holland, and X. W. Li (2014), Freeboard and mass extraction of the disintegrated Mertz Ice Tongue with remote sensing and altimetry data, *Remote Sens. Environ.*, *144*, 1–10.
Williams, G. D., and N. L. Bindoff (2003), Wintertime oceanography of the Adélie depression, *Deep Sea Res., Part II*, *50*(8), 1373–1392.
Williams, G. D., N. L. Bindoff, S. J. Marsland, and S. R. Rintoul (2008), Formation and export of dense shelf water from the Adélie Depression, East Antarctica, *J. Geophys. Res.*, *113*, C04039, doi:10.1029/2007JC004346.
Williams, G. D., S. Aoki, S. R. Rintoul, S. S. Jacobs, T. Tamura, and N. L. Bindoff (2010), Antarctic Bottom Water production along the Adélie and George V Land coast, East Antarctica (140–149°E), *J. Geophys. Res.*, *115*, C04027, doi:10.1029/2009JC005812.
Young, N., B. Legrésy, R. Coleman, and R. Massom (2010), Mertz Glacier tongue unhinged by giant iceberg, *Aust. Antarct. Mag.*, *18*, 19.